INSTITUTE OF PHYSICS PUBLISHING JOURNAL OF PHYSICS: CONDENSED MATTER

J. Phys.: Condens. Matter **14** (2002) 11671–11686 PII: S0953-8984(02)35201-9

Incommensurate phases in the improper ferroelastic $MgGeF_6{\cdot}6H_2O{:}Mn^{2+}$ studied by means of EPR

P G Skrylnik and A M Ziatdinov[1]

Institute of Chemistry, Far Eastern Branch of the Russian Academy of Sciences, 159, Prosp. 100-letiya, 690022 Vladivostok, Russia

E-mail: chemi@online.ru

Received 26 March 2002, in final form 30 July 2002
Published 1 November 2002
Online at stacks.iop.org/JPhysCM/14/11671

Abstract

The results of an EPR study of the inhomogeneous phases existing in the temperature interval $T_C = 311.0 \pm 0.3\,\mathrm{K} < T < T_{i1} = 403 \pm 0.3\,\mathrm{K}$ in improper ferroelastic crystals of $MgGeF_6{\cdot}6H_2O{:}Mn^{2+}$ are presented. On the basis of the analysis of the temperature and angle dependences of the experimental parameters and numerical calculations, the conclusion has been drawn that at T_{i1} the crystals considered undergo a transition to a structurally modulated phase and the order parameter of this transition may be the angle of the $Mg[H_2O]_6^{2+}$ octahedra rotation around the crystal C_3-axis. From T_{i1} to T_C the modes of the modulated phase follow according to a completely classical scenario for incommensurate crystals: the origin of the incommensurate structure with plane-wave modulation at T_{i1}, the appearance of structural phase solitons below $T_{i2} = 380 \pm 0.3$ K and decrease of the soliton density to values of $\approx$0.85 as the temperature decreases to $T \approx 360$ K. Below that temperature the soliton density is almost unchanged down to T_C and, to successfully describe the experimental spectra, the effect of variation of the spin–lattice relaxation rate over the spectrum has also been taken into account within the temperature interval considered. At T_C the crystals investigated undergo a first-order improper ferroelastic phase transition into a monoclinic phase with unit-cell doubling. A comparison with results on $MgSiF_6{\cdot}6H_2O$ from a previous investigation and a theoretical analysis of the structure evolution in these crystals are also presented.

1. Introduction

The crystals $MgGeF_6{\cdot}6H_2O{:}Mn^{2+}$ belong to the family $ABF_6{\cdot}6H_2O$ (where A and B are a divalent metal and a tetravalent element, respectively). They possess a wide variety of physical properties and are traditional objects of investigation for EPR spectroscopy [1–25].

[1] Author to whom any correspondence should be addressed.

In these compounds, complex $A[H_2O]_6^{2+}$ ions and $[BF_6]^{2-}$ octahedra form a rhombohedrally distorted CsCl-type lattice and can be distributed between two orientations around the threefold axis [26–38]. Many compounds of this family undergo an improper ferroelastic phase transition from the high-temperature rhombohedral phase to the low-temperature monoclinic phase [8, 9, 16, 28, 30–39]. Depending on the structure of the high-temperature phase, $ABF_6{\cdot}6H_2O$ crystals may be divided into two groups. The first one contains, for instance, fluorosilicates of Co, Ni and Zn [29, 34], in which crystals of the room temperature disordered structure with space group $R\bar{3}$ form, and two different orientations of $[BF_6]^{2-}$ ions rotated with respect to each other by some angle around the threefold crystal axis are present. The fluorosilicates of Mg, Fe and Mn belong to the second group. The presence of superstructure reflections at room temperature for these crystals, in contradiction to the structural model given by Hamilton [27] and Syoyama and Osaki [28], was the reason for Chevrier *et al* [31, 32, 35–38] introducing the space group $P\bar{3}$ for the proper treatment. Chevrier *et al* [31, 32, 35–38] also assumed two types of domain with different orientations of complex ions, connected by a pseudomirror plane (11.0). The analysis of the superstructure reflections shows that in the case of Mg and Mn compounds the sizes of the domains are nearly equal and quite large (∼300 Å) [31, 36], whereas in Fe fluorosilicate their sizes are temperature dependent [32]. The structural model given by Chevrier and Jehanno [31] for the $MgSiF_6{\cdot}6H_2O$ crystals above the temperature T_C of the improper ferroelastic phase transition (space group $P\bar{3}$) accounts for the observed superstructure reflections with periodic antiphase structure, built from ordered low-temperature monoclinic unit cells (space group $P2_1/c$) with integer period.

At present the data on the structure of magnesium hexahydrate hexafluorogermanate crystals are limited [40, 41]. According to x-ray single-crystal diffraction data given by Kouznetsov *et al* [40] at room temperature, the crystals considered have been assigned to space group $R\bar{3}$ ($Z = 1$). However, on the basis of a more recent and detailed structural investigation of single crystals, Stepien-Damm *et al* [41] reported that $MgGeF_6{\cdot}6H_2O$ crystals belong to the space group $P2_1/c$ ($Z = 2$) at room temperature. These authors pointed out the presence of a phase transition at ≈315 K from the monoclinic phase to the trigonal one with domain-like structure.

After the structurally inhomogeneous phase in $MgBF_6{\cdot}6H_2O$ (B = Si, Ge, Ti) crystals, existing between their rhombohedral paraelastic phase and their monoclinic ferroelastic one, had been discovered by Ziatdinov *et al* [12–15], most of the attention of interested researchers [12–15, 17–25] was attracted to the nature of this phase (hereafter in this paper called the 'intermediate' phase). For the interpretation of experimental data, various different models of the 'intermediate' phase in these crystals have been suggested: some modifications of the incommensurate structure model [12–15, 17–22], a model of static and dynamic disordered structure fragments [23, 24] and the domain model [25]. All of these models have been analysed by us previously, with application to $MgSiF_6{\cdot}6H_2O$ [42]. In this paper, on the basis of the analysis of $MgGeF_6{\cdot}6H_2O{:}Mn^{2+}$ single-crystal EPR experiments, we suggest a model of their structural organization in the 'intermediate' phase which relies on our previous ideas on the incommensurate structure of this phase [14, 21], but is free of some disadvantages of models formerly proposed assuming incommensurate modulation of lattice displacements in these crystals. The model presented allows a successful description of the experimental Mn^{2+} EPR spectra in their 'intermediate' phase.

2. Experimental details

The EPR measurements were carried out using an X-band spectrometer ESR-231 (produced in Germany) and a Q-band spectrometer RE-1308 (produced in Russia) in three mutually

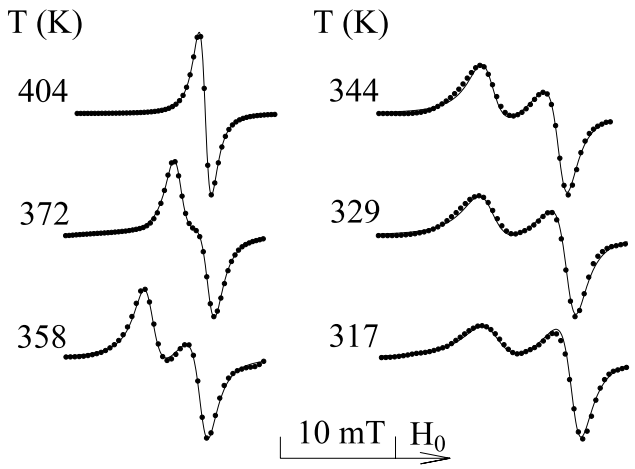

Figure 1. The temperature evolution of the Mn^{2+} EPR low-field HFS line for $MgGeF_6{\cdot}6H_2O{:}Mn^{2+}$ crystals at X-band and $\boldsymbol{H}_0 \parallel \boldsymbol{C}_3$. Dots and solid curves correspond to experimental and theoretical spectra, respectively.

perpendicular crystal planes. The orientation of the single crystal with respect to the direction of the external magnetic field $\boldsymbol{H}_0$ was varied with a two-axis goniometer system.

Single crystals of $MgGeF_6{\cdot}6H_2O$ doped with $\sim$0.1% Mn^{2+} ions have been grown from aqueous solution at room temperature according to the method which was used in [43]. The fluorogermanate powder was purchased commercially. The trigonal $\boldsymbol{C}_3$-axis in most of the samples in these experiments was readily identified by inspection and then it was identified as the [111] direction in cubic coordinates.

The temperature range of the experiments was 77–430 K. The crystal temperature variation was carried out by changing the temperature of a gaseous nitrogen flow passing through the quartz Dewar tube containing the crystal investigated. To monitor the temperature, copper–constantan thermocouples with base point at the ice melting temperature were used. The accuracy of the monitoring and the stability of the temperature were $\sim$0.3 K and $\sim$0.1 K h^{-1}, respectively.

3. Results

At temperature above $T_{i1} = 403.0 \pm 0.3$ K and for $\boldsymbol{H}_0 \parallel \boldsymbol{C}_3$ the EPR spectrum of $MgGeF_6{\cdot}6H_2O{:}Mn^{2+}$ crystals consists of 5×6 hyperfine-structure (HFS) lines. Analysis of the angular dependence of the spectrum in different planes demonstrates that it is of axial character with the z-axis parallel to the $\boldsymbol{C}_3$-axis and corresponds to one type of Mn^{2+} centre. The Mn^{2+} ($3d^5$, $S = 5/2$, $I = 5/2$) EPR spectrum is described by a conventional axial spin Hamiltonian with parameters as follows ($T \cong 415$ K):

$$g_\perp \cong g_\parallel = 2.0009 \pm 0.0003, \qquad D = (-265 \pm 1) \times 10^{-4}\ \mathrm{cm}^{-1},$$
$$a = (8 \pm 1) \times 10^{-4}\ \mathrm{cm}^{-1}, \qquad A_\perp \cong A_\parallel = (-89 \pm 1) \times 10^{-4}\ \mathrm{cm}^{-1}.$$

This Mn^{2+} spectrum is typical for the rhombohedral ($R\bar{3}$) phase of the crystals of the family considered [2, 7, 9, 16].

With temperature decrease below T_{i1}, all HFS spectral lines at first smoothly broaden and then, excluding the central set of lines corresponding to the $|1/2, m\rangle \leftrightarrow |-1/2, m\rangle$ transitions,

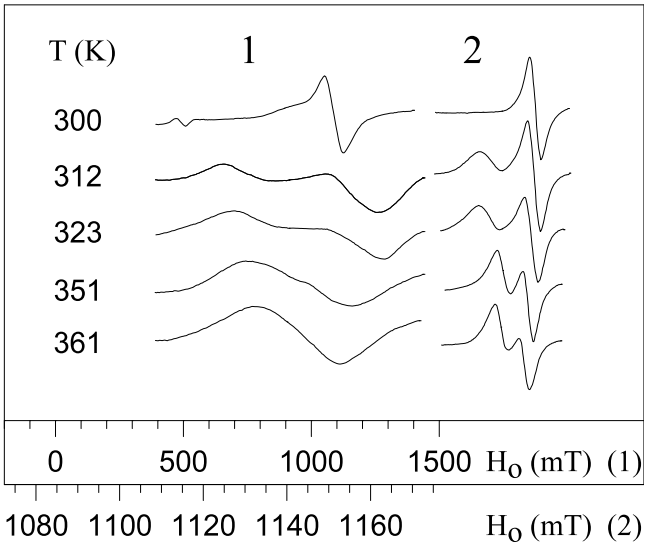

Figure 2. The temperature evolution of the Ni^{2+} fine-structure lineshape in the Q-band experiment (1) and, for comparison, the Mn^{2+} HFS low-field lineshape in the X-band experiment (2) on $MgGeF_6{\cdot}6H_2O$ crystals ($\boldsymbol{H}_0 \parallel \boldsymbol{C}_3$). The low-field line of small intensity in the Ni^{2+} spectrum corresponds to a 'forbidden' transition.

gradually transform into two-peak ones. In figure 1 such lineshape evolution is demonstrated for the low-field HFS line which was chosen for detailed analysis[2].

In spite of the substantial changes in Mn^{2+} HFS lineshapes below T_{i1}, the EPR spectrum symmetry and its principal axis direction remain the same. With temperature increase the reverse evolution of the Mn^{2+} EPR spectrum is observed. The temperature of transition from one spectrum type to another does not depend on the direction of temperature variation, the microwave field frequency, the orientation of $\boldsymbol{H}_0$ with respect to the crystal axes or the choice of HFS line for detecting the temperature changes in the sample. These features unambiguously demonstrate that T_{i1} is the second-order phase transition temperature, rather than the temperature of dynamic averaging on the EPR timescale of structurally inequivalent positions of complex ions. The temperature evolution of the EPR fine-structure lineshapes of Ni^{2+} admixture ions (figure 2) is qualitatively similar to that for Mn^{2+} spectral lines and the temperature of merging of the components of the fine-structure lines has been found to coincide with that obtained in EPR experiments with Mn^{2+} admixture ions.

At $T_{i2} = 380.0 \pm 0.3$ K, small stepwise changes with temperature hysteresis $\sim$1 K in the EPR spectra lineshape parameters (figure 3) are observed. It is worth noting that with temperature decreasing below T_{i2} the spectral lines transform into two components with different linewidths, preserving the spectral continuum between them; one component broadens with temperature decrease whereas the other is almost unchanged. However, despite substantial HFS lineshape changes below T_{i2}, the EPR spectrum symmetry and its principal axis direction remain invariant.

The temperature decrease below T_{i2} leads to a sequence of stepwise changes in slope of the temperature dependences of the lineshape parameters (figure 4). The temperature values of the slope discontinuities T_{in} ($n = 2$–5) depend on the direction of temperature change and

[2] A specially conducted investigation has proved that Mn^{2+} EPR signals from dehydrated regions of the crystal do not overlap with the chosen HFS line and, therefore, do not distort it over the entire temperature range of the study.

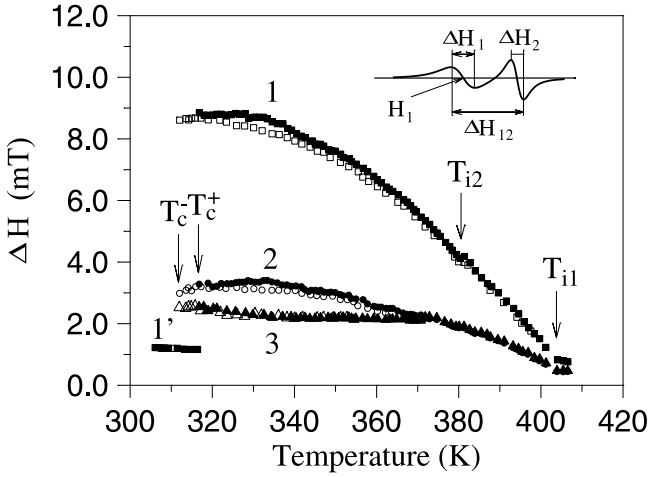

Figure 3. The temperature dependence of the Mn^{2+} EPR low-field HFS lineshape parameters for $MgGeF_6{\cdot}6H_2O{:}Mn^{2+}$ crystals at X-band and for $\boldsymbol{H}_0 \parallel \boldsymbol{C}_3$. 1: ΔH_{12}; 1′: linewidth in the ferroelastic phase; 2: ΔH_1; 3: $\Delta H2$. The black and white dots refer to parameters for heating and cooling of the crystals, respectively. The definitions of the lineshape parameters studied are presented too.

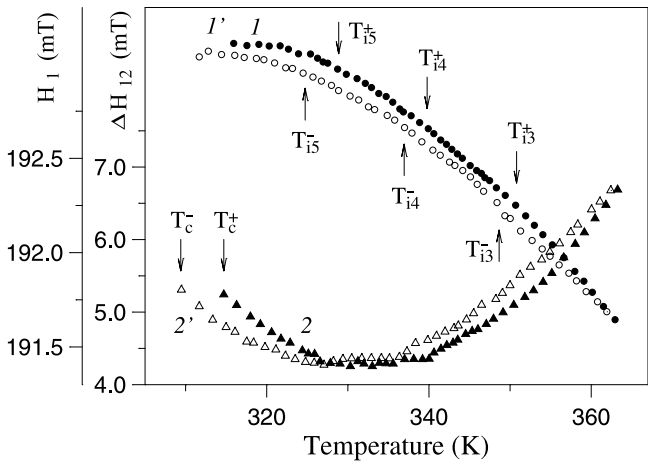

Figure 4. The temperature dependence of the Mn^{2+} EPR low-field HFS lineshape parameters (defined in figure 3, inset) for $MgGeF_6{\cdot}6H_2O{:}Mn^{2+}$ crystals at X-band and $\boldsymbol{H}_0 \parallel \boldsymbol{C}_3$. 1: ΔH_{12}; 2: H_1. The black (1 and 2) and white (1′ and 2′) dots refer to parameters for heating and cooling of the crystals, respectively.

vary from sample to sample within ∼4 K, but they occur at practically the same values of the lineshape parameters. The temperature dependence of the lineshape parameter H_1 (see figure 4) is of special importance for clearly detecting the T_{i4}- and T_{i5}-values, since significant changes in slope have been observed instead of small discontinuities. Additional experiments have been carried out to investigate hysteresis phenomena, observed from T_{i2} to T_C, in multiple heating/cooling cycles (figure 5) and at different depths in these cycles (figure 6). It was found that multiple cycling results in nearly the same temperature dependences, whereas different depths of temperature cycles cause apparent changes in these dependences, although the T_{in} were clearly detected in all cases.

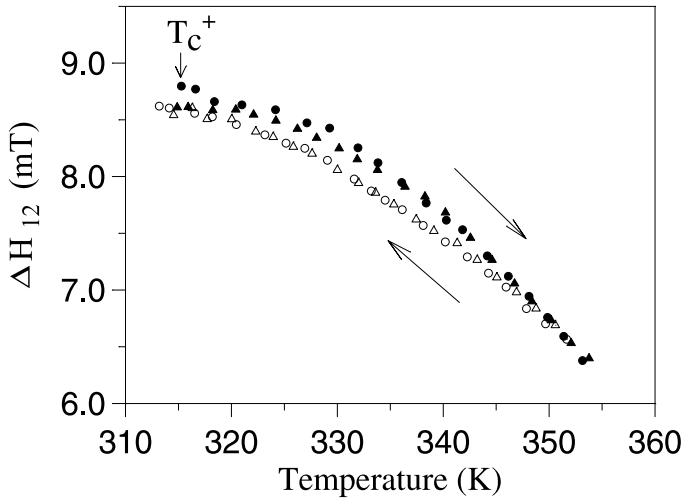

Figure 5. The temperature dependence of the Mn^{2+} EPR low-field HFS lineshape parameter ΔH_{12} for $MgGeF_6{\cdot}6H_2O{:}Mn^{2+}$ crystals (X-band, $\boldsymbol{H}_0 \parallel \boldsymbol{C}_3$) in multiple heating/cooling cycles. The black and white dots refer to values for heating and cooling of the crystals, respectively (triangles and circles correspond to different cycles).

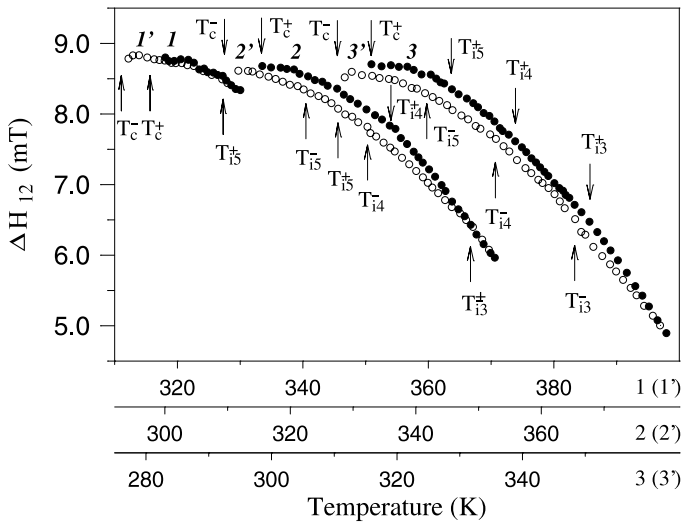

Figure 6. The temperature dependence of the Mn^{2+} EPR low-field HFS lineshape parameter ΔH_{12} for $MgGeF_6{\cdot}6H_2O{:}Mn^{2+}$ crystals (X-band, $\boldsymbol{H}_0 \parallel \boldsymbol{C}_3$) at different depths of the heating/cooling cycle. The black (1, 2 and 3) and white (1′, 2′ and 3′) dots refer to values for heating and cooling of the crystals, respectively.

At $T_C = 311.0 \pm 0.3$ K the $MgGeF_6{\cdot}6H_2O$ crystals undergo a first-order structural phase transition with the temperature hysteresis ∼3 K. Below T_C the EPR spectrum corresponds to six spatially inequivalent rhombic centres. It is worth noticing that analysis of the angular dependences and variation of the relative intensities of Mn^{2+} EPR lines (from sample to sample and from experiment to experiment for the sample) and investigation of the $MgGeF_6{\cdot}6H_2O$ crystal with a polarization microscope demonstrate that the crystal under study, below T_C,

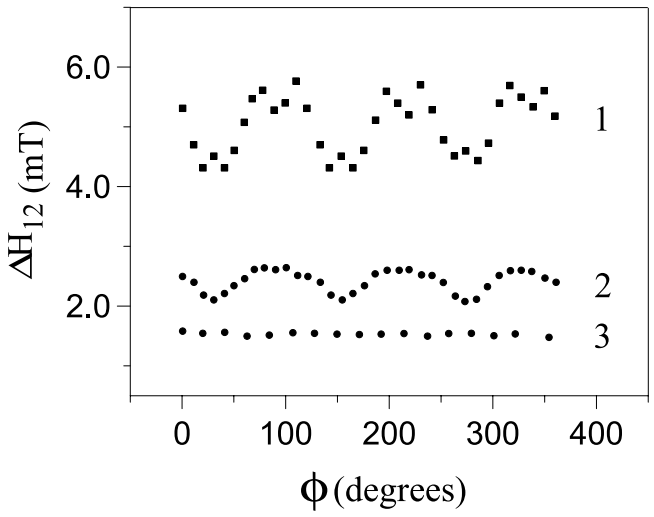

Figure 7. Angle dependences of the value of the Mn^{2+} EPR low-field HFS line splitting ΔH_{12} for $MgGeF_6{\cdot}6H_2O{:}Mn^{2+}$ crystals for rotation of the sample around the C_3-axis (around the ϕ-angle axis), which makes the angle $\theta \approx 50°$ with H_0, at different temperatures (curve 1 corresponds to 320 K, curve 2 to 380 K, curve 3 to 410 K). (For the X-band.)

consists of orientational domains of three kinds connected with each other by 120° rotation around C_3 and each domain contains two inequivalent rhombic Mn^{2+} sites. Therefore, $MgGeF_6{\cdot}6H_2O$ crystal undergoes an improper ferroelastic phase transition at T_C. At $H_0 \parallel C_3$ the linewidths of the Mn^{2+} HFS lines immediately after the phase transition are approximately the same as those immediately before the transition from the paraelastic to the 'intermediate' phase (figure 3).

Below T_C, the z-axis of each Mn^{2+} centre deviates by an angle of $(8 \pm 2)°$ with respect to the C_3-axis above T_C. The EPR spectra of all spatially inequivalent Mn^{2+} centres are in good agreement with the conventional rhombic spin Hamiltonian with the following parameters ($T \cong 250$ K):

$$g_\perp \cong g_{||} = 2.0009 \pm 0.0005,$$
$$D = (-253 \pm 2) \times 10^{-4}\ \mathrm{cm}^{-1}, \qquad |E| = (36 \pm 5) \times 10^{-4}\ \mathrm{cm}^{-1},$$
$$a = (8 \pm 2) \times 10^{-4}\ \mathrm{cm}^{-1}, \qquad A_\perp \cong A_{||} = (-92 \pm 1) \times 10^{-4}\ \mathrm{cm}^{-1}.$$

The number of Mn^{2+} sites and the symmetry of individual magnetic ion EPR spectra in the single structural domain of $MgGeF_6{\cdot}6H_2O{:}Mn^{2+}$ below T_C agree with the data from the single-crystal x-ray structural investigation [41], with the reported space group $P2_1/c$ below $\approx$315 K.

Within the temperature range from T_C to T_{i1}, upon rotation of the single crystal around C_3 (varying the azimuthal angle ϕ) which makes a certain angle $\theta \neq 0°, 90°$ with the H_0-direction, a 120° angular dependence of the Mn^{2+} EPR lineshape has been observed (figure 7). The amplitude for such variations in lineshape parameters increases with temperature decrease (figure 7).

At $T < T_{i2}$, the low-field broad component of the HFS line narrows when the polar angle θ tends to the 'magic' angle value (figure 8). Simultaneously, the high-field component of the HFS line broadens (figure 8). The components merge as θ tends to the 'magic' angle.

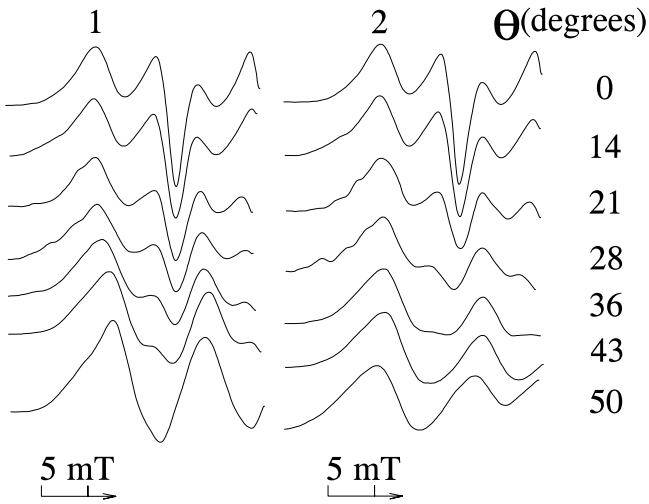

Figure 8. Angle dependences of the Mn^{2+} EPR low-field HFS lineshape for $MgGeF_6{\cdot}6H_2O{:}Mn^{2+}$ crystal for rotation around the θ-angle axis in the planes containing the C_3-axis. Columns 1 and 2 correspond to rotating the crystal in the planes in which ΔH_{12} takes maximal and minimal values, respectively. (For the X-band.)

4. Discussion

The shape of the Mn^{2+} HFS lines for $MgGeF_6{\cdot}6H_2O{:}Mn^{2+}$ (the presence of two edge singularities with a spectral continuum between them) and their evolution with temperature decrease from T_{i1} to T_C (increase in difference between the magnetic field values, corresponding to edge singularities with continuum conservation) are characteristic of magnetic resonance spectra of incommensurate structures with one-dimensional modulation of the lattice displacements [44, 45]. Note that the 'global' hysteresis phenomena observed over the entire temperature range from T_{i2} to T_C (figure 4) is also indirect evidence for the incommensurate nature of the 'intermediate' phase [46, 47].

Bearing in mind that the symmetry and principal axis direction of the Mn^{2+} EPR spectrum for $MgGeF_6{\cdot}6H_2O{:}Mn^{2+}$ do not change from T_{i1} to T_C, the θ-angle dependence of the lineshapes (decrease in difference between the resonance magnetic field values corresponding to components of HFS lines as θ tends to the 'magic' angle) and that the spread of the inhomogeneous HFS lines observed below T_{i1} occurs only when there is variation of the axial fine-structure parameter D, one may conclude that in the crystals investigated, at $T < T_{i1}$, the modulated lattice displacement is the trigonal distortion of $[Mn(H_2O)_6]^{2+}$ octahedra. Taking into account these facts and considerations, the analysis of the experimental data on the temperature and angular dependences of the EPR Mn^{2+} admixture ion spectra has been carried out within the framework of the model of incommensurate modulation.

In the general case, the incommensurate one-dimensional spatial modulation of the lattice displacements is determined by the following equation [48]:

$$u(x) = A(x)\cos[\varphi(x)], \tag{1}$$

where $A(x) = A_0 + \delta A(x)$ is the amplitude and $\varphi(x) = \Phi(x) + \Phi_0$ (Φ_0 is the initial phase shift) is the phase of the lattice displacements. In the plane-wave regime of modulation, $\delta A = 0$ and $\varphi(x)$ is a linear function of the spatial variable x (along the modulation direction). As a rule, with temperature decrease a transition from the plane-wave regime to the multisoliton one

(distortion of the phase and amplitude of the modulation wave) occurs [44, 45], resulting in the appearance of phase solitons and, further, amplitude solitons [48]. For the phase solitons, $A = A_0$ and the phase function $\varphi(x)$ becomes a non-linear function expressed using the solution of the one-dimensional sine–Gordon equation:

$$\frac{\partial^2\Phi(x)}{\partial x^2} = -\alpha^2 \sin[n\Phi(x)], \tag{2}$$

where $n = 2p$ [45], p is the superstructure multiplicity, α is a constant determined by the soliton density n_S. According to Blinc *et al* [45], $n_S = 2\pi/(nd\varphi'_{max})$, with d being equal to the distance between the solitons and φ'_{max} the maximum value of the phase function derivative. With further decrease of temperature the amplitude variations $\delta A(x)$ may become significant, resulting in amplitude solitons appearing. At $\delta A \ll A_0$, the function $A(x)$ is determined by the approximate expression [45]

$$\frac{\partial A(x)}{\partial x} \approx -C\frac{\partial^2\Phi(x)}{\partial x^2}, \qquad C > 0. \tag{3}$$

It is worth noting that, in many experimental cases, amplitude solitons are not observed and the multisoliton lattice may be well described in the framework of the $A(x) = A_0$ approximation, i.e. within the phase soliton approximation. The soliton density decreases with temperature decrease down to the temperature of transition to the commensurate state (the 'lock-in' transition). However, within some temperature range below T_C, the soliton density may remain at a non-zero value [45].

In the incommensurate phase the resonance magnetic field H_r for a certain paramagnetic centre is a function of the small-lattice-displacement parameter $u(x)$. It may be expanded into a power series:

$$H_r = H_{r0} + h_1(x)\cos[\varphi(x)] + h_2(x)\cos^2[\varphi(x)] + \cdots, \tag{4}$$

where the h_i are the constant values for the plane-wave and phase soliton regimes. The resulting spectrum shape may be calculated by integration over possible H_r-values using some single lineshape (Lorentzian in most cases) for a certain H_r.

In the crystals under investigation, every paramagnetic ion is situated on the symmetry axis and at an inversion centre simultaneously. Therefore, according to symmetry consideration [45], for $\boldsymbol{H}_0 \parallel \boldsymbol{C}_3$, only even terms in equation (4) should be retained. This conclusion may be drawn from microscopical considerations as well. Because of the special importance of the correct choice of expansion (4) for the subsequent experimental data analysis, this consideration is presented below in detail.

The appearance of the ϕ-angle dependence of the EPR lineshape in $MgGeF_6{\cdot}6H_2O{:}Mn^{2+}$ crystals below T_{i1} (figure 7) is evidence for the appearance of misorientation of cubic crystal field axes on different Mn^{2+} ions, i.e. rotation of the complex ions $Mg[H_2O]_6^{2+}$ around the trigonal axis in the incommensurate phase. The amplitude of this misorientation increases with temperature decrease. Also, in the ferroelastic phase, within each orientational domain, two spatially inequivalent complexes $Mg[H_2O]_6^{2+}$, rotated with respect to each other around the $\boldsymbol{C}_3$-axis by a certain angle, are present [14, 21]. The facts stated above allow us to conclude that the angle $\delta\phi$ of the rotation of the octahedra $Mg[H_2O]_6^{2+}$ around the trigonal axis with respect to their position in the paraelastic phase can be a primary order parameter of the paraelastic–incommensurate phase transition in $MgGeF_6{\cdot}6H_2O$. (Obviously, the trigonal distortion of the octahedra $Mg[H_2O]_6^{2+}$ with respect to their distortion in the paraelastic phase cannot be a primary order parameter of this transition, because such an assumption leads to at least two $Mg[H_2O]_6^{2+}$ configurations with different values of the trigonal distortion (and D-values) in the ferroelastic phase, which does not agree with the EPR [14, 21] and x-ray [41] data.)

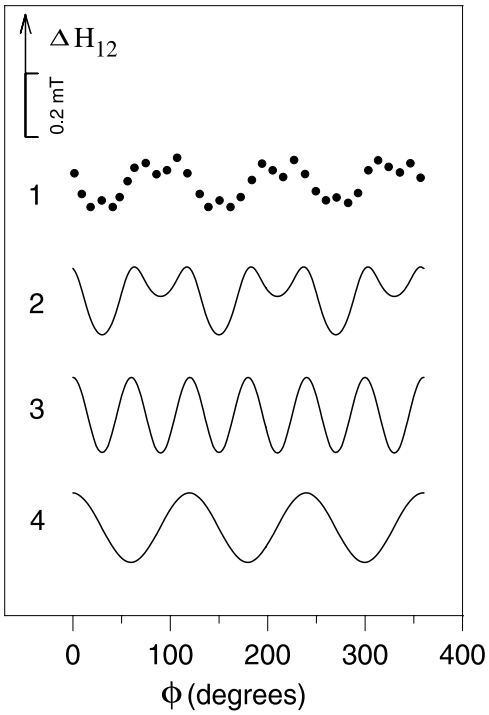

Figure 9. The dependence of the Mn^{2+} EPR lineshape parameter ΔH_{12} on the ϕ-angle for $MgGeF_6{\cdot}6H_2O{:}Mn^{2+}$ crystals. Dots (labelled 1) correspond to experiment (the X-band; $\boldsymbol{H}_0 \parallel \boldsymbol{C}_3$). Solid curves correspond to calculated dependences (2: the model of quadratic modulation of the D-parameter $\delta D = d_2\phi^2$, $\phi(x) = \delta\phi_x \cos(x)$, $\delta\phi_1 = 7°$, $d_2 = 0.121 \times 10^{-4}$ cm^{-1} deg^{-2}; 3: the model of two discrete octahedra orientations: $\delta\phi = 5°$; 4: the model of linear modulation of the D-parameter $\delta D = d_1\phi$, $\phi(x) = \delta\phi_1 \cos(x)$, $\delta\phi_1 = 1.2°$, $d_1 = 2.470 \times 10^{-4}$ cm^{-1} deg^{-1}).

Taking that into consideration, we may suppose that the stepwise peculiarities in the slope of the dependences of the EPR lineshape parameters versus temperature are associated with the discontinuities in the slope of the temperature dependence of the rotations of the $Mg[H_2O]_6^{2+}$ octahedra around the $\boldsymbol{C}_3$-axis.

Further, one may suppose that the rotation of octahedra around the trigonal axis, as a consequence of the change in lengths and orientations of the hydrogen bonds, is accompanied by a change in the trigonal distortion of the complexes and, therefore, by variation of the fine-structure parameter, i.e. $D = D_0(T) + \Delta D(\delta\phi)$, where $D_0(T)$ is the value of the fine-structure parameter for a complex not distorted by a modulation wave and $\Delta D(\delta\phi)$ is a contribution to the fine-structure parameter caused by modulated distortion. For reasons of symmetry (the presence of a symmetry axis and inversion centres), one can draw the conclusion that $\Delta D(\delta\phi)$ is an even function. Hence, neglecting modulation of other spin Hamiltonian parameters, series (4) for $\boldsymbol{H}_0 \parallel \boldsymbol{C}_3$ should contain only even terms (in this orientation, H_r does not directly depend on the crystalline cubic axis orientation). The conclusion reached is consistent with the data on the ϕ-dependence of the Mn^{2+} HFS lineshape analysis also. Below T_{i1} this dependence may be qualitatively described only within the framework of the model of quadratic modulation of the D-parameter connected with trigonal lattice distortions (figure 9 demonstrates that the model of linear modulation of the D-parameter, like the model of two discrete octahedra orientations, results in clear qualitative differences from the experimental dependence).

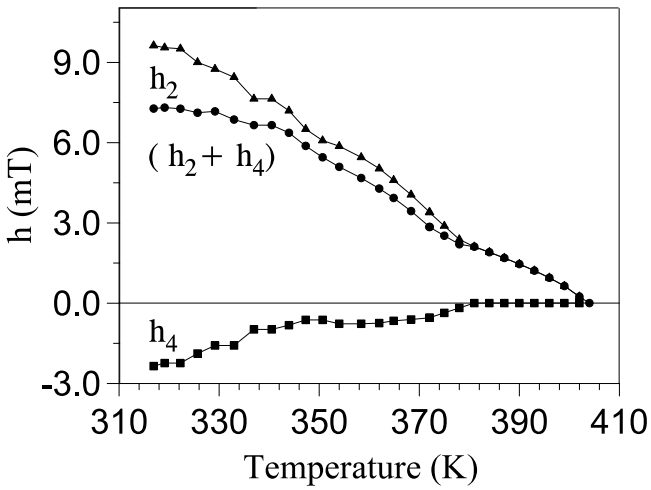

Figure 10. The temperature dependence of the incommensurate modulation parameters of second (h_2) and fourth (h_4) order calculated from the experimental Mn^{2+} EPR low-field HFS line for $MgGeF_6{\cdot}6H_2O{:}Mn^{2+}$ crystals at the X-band and for $\boldsymbol{H}_0 \parallel \boldsymbol{C}_3$. Solid curves connecting dots are present for convenience only.

Therefore, both from general symmetry considerations and from microscopic ones, for the crystal investigated for $\boldsymbol{H}_0 \parallel \boldsymbol{C}_3$, equation (4) is reduced as follows:

$$H_r = H_{r0} + h_2(x)\cos^2[\varphi(x)] + h_4(x)\cos^4[\varphi(x)] + \cdots. \tag{5}$$

Using (5) we were able to describe the Mn^{2+} HFS lineshapes well, within the temperature range from T_{i1} to ≈370 K (figure 1). Moreover, close to T_{i1} the HFS lineshape is similar to the symmetric one and, as consequence, the h_4-value is small and the spectra may be described with good accuracy taking into account just the quadratic modulation term (figure 10).

Below ≈370 K a good description of the experimental spectra is possible only on introducing the phase solitons; i.e. upon cooling below $T \approx 370$ K, the plane-wave regime of modulation transforms into the multisoliton one. In the absence of phase transitions between T_{i1} and T_C, if the direction of one-dimensional modulation coincides with the direction of multiple increase of the unit cell in the ferroelastic (ferroelectric) phase with respect to that of the paraelastic (paraelectric) phase, the value of p is assumed to be equal to this multiplicity [44]. According to the EPR results presented (see section 3) and structural data [41] on the ferroelastic phase of $MgGeF_6{\cdot}6H_2O$, the unit-cell size is doubled in the direction of the monoclinic $\boldsymbol{b}_m$-axis (which is perpendicular to the trigonal axis in the para-phase) compared to the paraelastic phase. Therefore, in this case the analysis should be carried out for the multisoliton regime with $n = 4$. The corresponding calculation provides a good description of experimental spectra below ≈370 K (see figure 1). It is worth noticing that the character of the temperature dependences of the EPR lineshape parameters (see figures 4 and 6) indicates the possibility of structural phase transitions between T_{i1} and T_C. The phase transitions at T_{in} may be connected with the change in modulated phases, representing the 'devil's staircase' phenomenon [49]. In such a case the value of the n-parameter in equation (2) should change within the temperature range from T_{i1} to T_C. Unfortunately, this problem cannot be solved for the crystals considered by analysis of EPR data only, due to large soliton density ($n_S > 0.85$) down to T_C (for this reason, the experimental spectra are successfully described with values of n different from 4 ($n = 6$, for instance) as well).

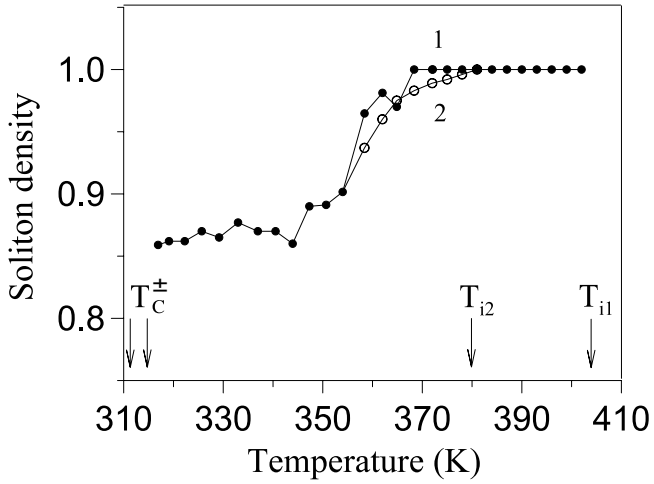

Figure 11. The temperature dependence of the soliton density n_S calculated on introducing solitons at $T \approx 370$ K (curve 1) and at $T \approx 380$ K (curve 2) for the model taking into account variation of T_1^{-1} over the Mn^{2+} EPR low-field HFS line for $MgGeF_6{\cdot}6H_2O{:}Mn^{2+}$ crystals. For the X-band. Solid curves connecting dots are present for convenience only.

We should note that in the related crystals $MgSiF_6{\cdot}6H_2O$, at T_{i2} qualitative changes in the EPR spectra parameters occur and the soliton density shows a stepwise decrease. In $MgGeF_6{\cdot}6H_2O$, a small discontinuity in ΔH_{12} has been observed at T_{i2} also, but there are no qualitative changes in the spectra at that temperature. In calculations for the latter crystals, a value of n_S different from unity may be used immediately below $T_{i2} \approx 380$ K (see figure 11, curve 2, for instance), with the same good agreement of calculated and experimental spectra being obtained in the two cases ($n_S \neq 1$ and $n_S = 1$). Therefore, there is no confirmation of the stepwise nature of the appearance of the soliton lattice at ≈370 K, but it should be taken into account below that temperature to describe the experimental spectra correctly.

Below ≈360 K a difference between the experimental spectra and theoretical curves calculated within the framework of the above model of lattice displacement modulation appears and it increases as temperature decreases (figure 12, curve 1). Hence, the model for the calculation should be more comprehensive. According to the data from theoretical studies of classical incommensurate systems at $T \to T_C$, significant amplitude variations of the order parameter may result in amplitude solitons appearing [48]. But below ≈360 K for the crystals investigated, calculations of spectral lineshapes taking into account the amplitude soliton effect have not led to a successful description of the experimental spectra (figure 12, curve 2).

Another approach has been suggested by Zapart and Zapart [25] for describing EPR spectra of $MgSiF_6{\cdot}6H_2O{:}Mn^{2+}$. According to that model, the periodic antiphase domain structure with a temperature-dependent width of the antiphase domains is realized. However, the calculated HFS lineshapes both for $MgSiF_6{\cdot}6H_2O{:}Mn^{2+}$ [25] and for the crystals considered (figure 12, curve 3) are far from the ones observed in experiment, also.

Theoretical [45] and experimental [50, 51] studies of the spin–lattice relaxation rate T_1^{-1} in incommensurate systems demonstrate that T_1^{-1} may vary considerably over the incommensurate spectral distribution. The amplitude of this variation increases with temperature decrease. The authors of the aforementioned papers account for the T_1^{-1}-variation over the incommensurate continuum by the difference in contributions of phasons and amplitudons to the effective spin–lattice relaxation rate. On the basis of these results we

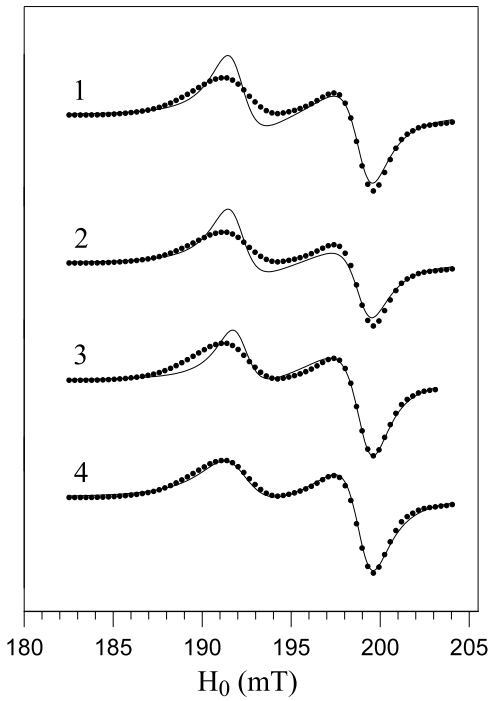

Figure 12. Comparison of the theoretical spectra, calculated within the frameworks of different models (solid curves), with the experimental spectrum (dots) for $MgGeF_6{\cdot}6H_2O{:}Mn^{2+}$ at 329 K (the X-band, $\boldsymbol{H}_0 \parallel \boldsymbol{C}_3$). 1: the model of incommensurate modulation: $h_2 = 8.73$ mT, $h_4 = -1.58$ mT, $W = 1.46$ mT, $n_S = 0.865$; 2: the model of incommensurate modulation with amplitude solitons: $h_2 = 8.75$ mT, $h_4 = -1.56$ mT, $W = 1.46$ mT, $n_S = 0.865$, parameter of amplitude modulation (amplitude variation maximum) $\delta A = 5\%$; 3: the domain model by Zapart and Zapart [25]: $h_2 = 7.64$ mT, percentage contribution of domain wall volume with respect to crystal volume 48.7%, $W = 1.37$ mT; 4: the model of incommensurate modulation with variation of the spin–lattice relaxation rate over the spectrum: $h_2 = 8.73$ mT, $h_4 = -1.58$ mT, $n_S = 0.865$, $W_0 = 2.21$ mT, $W_2 = 1.47$ mT, $\delta W = 0.07$ mT.

have conducted a simulation of experimental lineshapes, assuming a dependence of T_1^{-1} on the resonance magnetic field in magnesium fluorogermanate too. The calculations have been carried out assuming a parabolic dependence of the EPR linewidth W on the resonance magnetic field (figure 13, inset). Within the framework of this model, we have achieved a successful description of the experimental spectra below 360 K down to T_C (figure 1). The calculated soliton density at these temperatures varies by about 0.85 (figure 11). Over the entire range of the inhomogeneous phase, the value of the linewidth variation indicated remains reasonable (figure 13).

It is worth comparing the results of the theoretical analysis of the EPR spectra evolution for the fluorogermanate crystals presented in this paper and for the fluorosilicate ones [42]. In the case of $MgSiF_6{\cdot}6H_2O$ below $T_{i2} = 343$ K the soliton density falls to small values $n_S \approx 0.1$; the incommensurate spectral continuum near disappears and two single components appear instead; the variation of the spin–lattice relaxation rate over the spectrum becomes inexplicably large as the temperature decreases to T_C. These facts motivated us to propose the model of an inhomogeneous phase with two types of nearly independent region (domain-like ordered and soliton-like disordered regions) in the fluorosilicate crystals below T_{i2} [42]. In contrast, for $MgGeF_6{\cdot}6H_2O$ the calculations result in significant values of the soliton density $\approx$0.85;

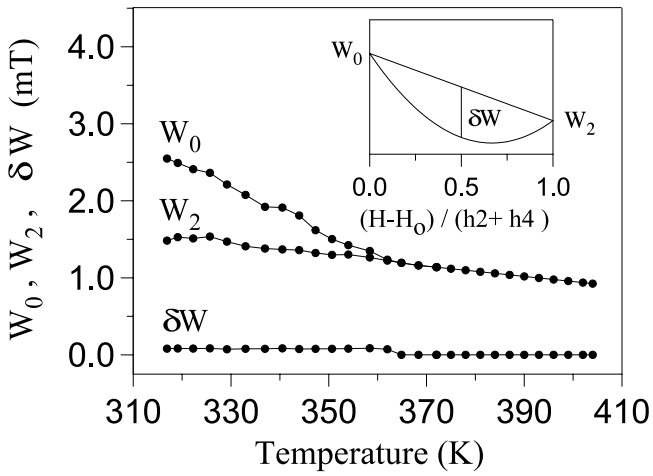

Figure 13. The temperature dependences of the parameters W_0, W_2 and δW calculated for the Mn^{2+} EPR low-field HFS line for $MgGeF_6{\cdot}6H_2O{:}Mn^{2+}$ crystals at the X-band and for $\boldsymbol{H}_0 \parallel \boldsymbol{C}_3$. The parameters W_0 and W_2 indicate the value of the Lorentzian linewidth at the points of incommensurate spectral singularities; δW is the deviation of the proposed parabolic dependence $W(H)$ from a linear function (inset). Solid lines connecting dots are present for convenience only.

the incommensurate spectral continuum is preserved; the variation of T_1^{-1} over the spectrum takes physically reasonable values. Therefore, one may conclude that the entire 'intermediate' phase in $MgGeF_6{\cdot}6H_2O$ crystals is an incommensurate phase (representing the analogue of the $MgSiF_6{\cdot}6H_2O$ structure evolution above 343 K), which is successfully described within the framework of the model presented. We should note, however, that admission of some statistical structural disorder of the trigonal distortions of $Mg[H_2O]_6^{2+}$ complexes in $MgGeF_6{\cdot}6H_2O$ crystals near T_C allows a good description of the experimental lineshapes with lower values of the linewidth variation compared to those for the results presented in figure 13.

Thus, the model of the $MgGeF_6{\cdot}6H_2O{:}Mn^{2+}$ crystal structure from T_{i1} to T_C considered above results in successful approximation of the experimental Mn^{2+} EPR spectra. The EPR method has advantages with respect to standard structural methods such as the x-ray diffraction technique, since it is exceptionally sensitive to the local structure of the samples investigated. This feature enabled us to detect and study disordered regions in $MgGeF_6{\cdot}6H_2O$ crystals and their transformation with temperature variation.

5. Conclusions

In the present paper, on the basis of EPR data for $MgGeF_6{\cdot}6H_2O{:}Mn^{2+}$ single crystals, structural organization motifs for their 'intermediate' phase, between monoclinic and rhombohedral ones ($T_C = 311 \pm 0.3$ K $< T < T_{i1} = 403 \pm 0.3$ K), are proposed. It is shown that at T_{i1} the crystals considered undergo a transition to a structurally modulated phase which may be an incommensurate phase. The primary order parameter of the paraelastic–incommensurate phase transition may be angle of the $Mg[H_2O]_6^{2+}$ octahedra rotation around the crystal $\boldsymbol{C}_3$-axis. Upon cooling below $T \approx 380$ K, the plane-wave regime of modulation transforms into the multisoliton one with the structural soliton density decreasing as long as the temperature decreases. Below $T \approx 360$ K the effect of variation of the spin–lattice relaxation rate over the spectrum has been taken into account, resulting in successful description of the experimental

spectra down to T_C. As against the formerly proposed models of structural organization of $MgGeF_6{\cdot}6H_2O$ crystals in the 'intermediate' phase, the model presented in this paper agrees with all known experimental data and does not contradict symmetry reasoning.

Acknowledgments

The authors would like to thank Professor R L Davidovich and Dr T F Antohina for providing us with the $MgGeF_6{\cdot}6H_2O$ crystals and Dr V G Kuryavyi for help in the EPR measurements.

References

[1] Holden A N, Kittel C and Yager W A 1949 *Phys. Rev.* **75** 1443
[2] Bleaney B and Ingram D J E 1951 *Proc. R. Soc.* A **205** 336
[3] Walsh W W 1959 *Phys. Rev.* **114** 1473
[4] Rubins R S 1962 *Proc. Phys. Soc.* **80** 224
[5] Altshuler S A and Valishev R M 1965 *Sov. Phys.–JETP* **48** 464
[6] Lukin S N and Tsintsadze G A 1975 *Sov. Phys.–JETP* **69** 250
[7] Zaripov M M, Ziatdinov A M, Yablokov Yu V and Davidovich R L 1975 *Sov. Phys.–Solid State* **17** 1164
[8] Ziatdinov A M, Zaripov M M, Yablokov Yu V and Davidovich R L 1976 *Phys. Status Solidi* b **78** K69
[9] Zaripov M M, Ziatdinov A M, Yablokov Yu V and Davidovich R L 1977 *Chem. Phys. Lett.* **48** 443
[10] Rubins R S and Kwee K K 1977 *J. Chem. Phys.* **66** 3948
[11] Hrabanski R, Sczaniecki P B and Stankowski J 1979 *Phys. Status Solidi* b **51** 243
[12] Ziatdinov A M, Kuryavyi V G and Davidovich R L 1985 *Sov. Phys.–Solid State* **27** 1288
[13] Ziatdinov A M, Kuryavyi V G and Davidovich R L 1986 *Sov. Phys.–Solid State* **28** 3549
[14] Ziatdinov A M, Kuryavyi V G and Davidovich R L 1987 *Sov. Phys.–Solid State* **29** 215
[15] Ziatdinov A M, Kuryavyi V G and Davidovich R L 1988 *Sov. Phys.–Solid State* **30** 3183
[16] Rubins R S, Drumheller J E and Hutton S L 1989 *J. Chem. Phys.* **91** 3614
[17] Hrabanski R 1991 *Ferroelectrics* **124** 333
[18] Suhara M, Bandoh T, Kitai T, Kobayashi T and Katsuda H 1992 *Phase Transit.* **37** 111
[19] Ziatdinov A M and Kuryavyi V G 1993 *Ferroelectrics* **143** 99
[20] Hrabanski R, Kapustianik V, Kardash V and Sveleba S 1994 *Phys. Status Solidi* a **142** 509
[21] Ziatdinov A M and Kuryavyi V G 1994 *Ferroelectrics* **156** 395
[22] Skrylnik P G and Ziatdinov A M 1999 *Bull. Magn. Reson.* **20** 39
[23] Hrabanski R and Kassiba A 1995 *Ferroelectrics* **172** 443
[24] Kassiba A, Hrabanski R, Bonhomme D and Hader A 1995 *J. Phys.: Condens. Matter* **7** 3339
[25] Zapart W and Zapart M B 1999 *Bull. Magn. Reson.* **19** 34
[26] Pauling L 1930 *Z. Kristallogr.* **72** 482
[27] Hamilton W C 1962 *Acta Crystallogr.* **15** 353
[28] Syoyama S and Osaki K 1972 *Acta Crystallogr.* B **28** 2626
[29] Ray S, Zalkin A and Templeton D H 1973 *Acta Crystallogr.* B **29** 2741
[30] Jehanno G and Varret F 1975 *Acta Crystallogr.* A **31** 857
[31] Chevrier G and Jehanno G 1979 *Acta Crystallogr.* A **35** 912
[32] Chevrier G, Hardy A and Jehanno G 1981 *Acta Crystallogr.* A **37** 578
[33] Price D E 1987 *Can. J. Phys.* **65** 1280
[34] Chattopadhyay T, Devreux F, Peters K, Peters E-M, Gmelin E and Ghosh B 1988 *J. Phys. C: Solid State Phys.* **21** 1321
[35] Chevrier G and Saint-James R 1990 *Acta Crystallogr.* C **46** 186
[36] Chevrier G 1991 *Acta Crystallogr.* B **47** 224
[37] Chevrier G 1992 *J. Solid State Chem.* **99** 276
[38] Chevrier G 1994 *J. Solid State Chem.* **111** 322
[39] Flerov I N, Gorev M V, Aleksandrov K S and Afanasyev M L 1992 *J. Phys.: Condens. Matter* **4** 91
[40] Kouznetsov V G, Gorbunova Yu E, Kozmin P A and Kovaleva E S 1968 *Zh. Strukt. Khim.* **9** 471
[41] Stepien-Damm J, Lukaszewicz K and Hrabanski R 1996 *Z. Kristallogr.* **211** 936
[42] Skrylnik P G and Ziatdinov A M 2001 *Ferroelectrics* **249** 279
[43] Tananaev I V and Avduevskaya K A 1960 *Zh. Neorg. Khim.* **5** 63
[44] Blinc R 1981 *Phys. Rep.* **79** 331

[45] Blinc R, Prelovsek P, Rutar V, Seliger J and Zumer S 1986 *Incommensurate Phases in Dielectrics* vol 2, ed R Blinc and A P Levanyuk (Amsterdam: North-Holland) pp 143–276
[46] Blinc R 1988 *Phase Transit.* **11** 255
[47] Jamet J P 1988 *Phase Transit.* **11** 335
[48] Bruce A D and Cowley R A 1981 *Structural Phase Transitions* (London: Taylor and Francis) p 407
[49] Bak P 1982 *Rep. Prog. Phys.* **45** 587
[50] Zumer S and Blinc R 1981 *J. Phys. C: Solid State Phys.* **14** 465
[51] Blinc R, Apih T, Dolinsek J and Mikac U 1995 *Phys. Rev.* B **51** 1354